GEOPHYSICS, VOL. 76, NO. 3 (MAY-JUNE 2011); P. WA13–WA21, 15 FIGS.
10.1190/1.3569799

Correction for the influence of velocity lenses on nonhyperbolic moveout inversion for VTI media

Mamoru Takanashi[1] and Ilya Tsvankin[1]

ABSTRACT

Nonhyperbolic moveout analysis plays an increasingly important role in velocity model building because it provides valuable information for anisotropic parameter estimation. However, lateral heterogeneity associated with stratigraphic lenses such as channels and reefs can significantly distort the moveout parameters, even when the structure is relatively simple. We analyze the influence of a low-velocity isotropic lens on nonhyperbolic moveout inversion for horizontally layered VTI (transversely isotropic with a vertical symmetry axis) models. Synthetic tests demonstrate that a lens can cause substantial, laterally varying errors in the normal-moveout velocity (V_{nmo}) and the anellipticity parameter η. The area influenced by the lens can be identified using the residual moveout after the nonhyperbolic moveout correction as well as the dependence of errors in V_{nmo} and η on spreadlength. To remove such errors in V_{nmo} and η, we propose a correction algorithm designed for a lens embedded in a horizontally layered overburden. This algorithm involves estimation of the incidence angle of the ray passing through the lens for each recorded trace. With the assumption that lens-related perturbation of the raypath is negligible, the lens-induced traveltime shifts are computed from the corresponding zero-offset time distortion (i.e., from "pull-up" or "push-down" anomalies). Synthetic tests demonstrate that this algorithm substantially reduces the errors in the effective and interval parameters V_{nmo} and η. The corrected traces and reconstructed "background" values of V_{nmo} and η are suitable for anisotropic time imaging and producing a high-quality stack.

INTRODUCTION

Kinematics of P-wave propagation in VTI media are governed by the vertical velocity V_0 and the Thomsen parameters ε and δ (Tsvankin and Thomsen, 1994). P-wave reflection traveltime in laterally homogeneous VTI media above a horizontal or dipping reflector depends only on two combinations of these parameters — the normal-moveout velocity V_{nmo} of horizontal events and the anellipticity parameter η (Alkhalifah and Tsvankin, 1995; Tsvankin, 2005):

$$V_{\mathrm{nmo}} = V_0\sqrt{1+2\delta}\,, \tag{1}$$

$$\eta = \frac{\varepsilon-\delta}{1+2\delta}\,. \tag{2}$$

The parameters V_{nmo} and η, which control all P-wave time-processing steps, can be obtained from nonhyperbolic moveout for horizontal reflectors or dip-dependent NMO velocity. In particular, the nonhyperbolic moveout equation introduced by Alkhalifah and Tsvankin (1995) has been widely used for estimating V_{nmo} and η in layered VTI media and building interval anisotropic velocity models (Alkhalifah, 1997; Grechka and Tsvankin, 1998; Alkhalifah and Rampton, 2001; Tsvankin, 2005).

Nonhyperbolic moveout analysis is conventionally performed under the assumption that the overburden is laterally homogeneous on the scale of spreadlength. However, even gently dipping structures often contain velocity lenses such as channels and carbonate reefs with thickness between 50 m and 200 m and width smaller than the maximum source-receiver offset of a typical seismic survey (Armstrong et al., 2001; Fujimoto et al., 2007; Takanashi et al., 2008; Jenner, 2009; see Figure 1). For isotropic media, lateral heterogeneity of this type has been recognized as one of the sources of the difference between the moveout and true medium velocities (Al-Chalabi, 1979; Lynn

Manuscript received by the Editor 29 July 2010; revised manuscript received 8 October 2010; published online 23 May 2011.
[1]Colorado School of Mines, Department of Geophysics, Center for Wave Phenomena, Golden, Colorado, U.S.A. E-mail: mtakanas@mines.edu; ilya@dix.mines.edu.

and Claerbout, 1982; Toldi, 1989; Blias, 2009). Such lens-induced errors in V_{nmo} lead to depth misties between seismic and well data (Fujimoto et al., 2007).

Although the moveout parameters (especially η) were shown to be sensitive to correlated traveltime errors (Grechka and Tsvankin, 1998), overburden heterogeneity is seldom taken into account in nonhyperbolic moveout inversion. Grechka (1998) shows analytically that a constant lateral velocity gradient does not substantially distort the estimates of V_{nmo} and η, as long as anisotropy and lateral heterogeneity are weak. The second and fourth horizontal velocity derivatives, however, can cause errors in V_{nmo} and η. Still, Grechka's (1998) results are limited to a single horizontal layer with smooth velocity variation and cannot be directly applied to models with thin lenses and other velocity discontinuities.

Fujimoto et al. (2007) and Fruehn et al. (2008) employ isotropic traveltime tomography to estimate the velocity inside the lens and remove the lens-induced velocity errors. Their case studies show the importance of integrating seismic and geologic information and understanding the relationship between the overburden heterogeneity and velocity errors. In the presence of anisotropy, the laterally varying velocity field can be reconstructed using anisotropic reflection tomography (e.g., Woodward et al., 2008). However, if the lens location is unknown, lens-induced traveltimes shifts can hinder accurate parameter estimation for layers underneath the lens.

In this paper, we study the influence of velocity lenses on nonhyperbolic moveout inversion for 2D VTI models. Lens-induced distortions are examined by performing finite-difference modeling of long-spread P-wave reflections and applying moveout inversion with the Alkhalifah-Tsvankin (1995) nonhyperbolic equation. We show that even a relatively thin velocity lens may cause pronounced errors in the moveout parameters V_{nmo} and η and describe several criteria for identifying the range of common-midpoint (CMP) locations, for which reflected rays cross the lens. To remove lens-induced traveltime shifts, we propose a correction algorithm that requires minimal a priori information. Synthetic tests demonstrate that this algorithm suppresses lens-related distortions on the stacked section and substantially reduces errors in the effective and interval parameters V_{nmo} and η.

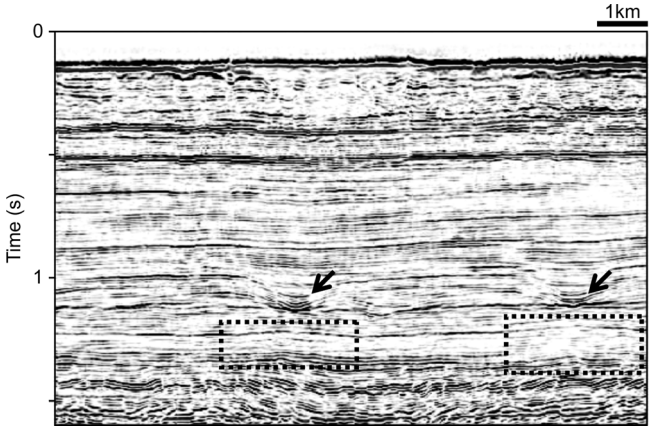

Figure 1. Time-migrated full-offset stacked section from the central North Sea (after Armstrong et al., 2001). Amplitude anomalies at the bottom of the channel-like structures (arrows) and pull-up anomalies below the structures (inside the rectangles) indicate the presence of lateral heterogeneity associated with the channel fills. Pull-up and push-down anomalies caused by high and low velocities, respectively, in channels or carbonate reefs are also observed in other hydrocarbon-producing regions, such as the Middle East and Northwest Australia.

DISTORTIONS CAUSED BY VELOCITY LENSES

To generate synthetic data, we perform finite-difference simulations (second-order in time, fourth-order in space) and anisotropic ray tracing for 2D models that include a low-velocity isotropic lens embedded in a horizontally layered VTI medium. The parameters V_{nmo} and η are estimated from nonhyperbolic moveout inversion based on the Alkhalifah-Tsvankin (1995) equation:

$$t^2 = t_0^2 + \frac{x^2}{V_{nmo}^2} - \frac{2\eta x^4}{V_{nmo}^2\left[t_0^2 V_{nmo}^2 + (1+2\eta)x^2\right]}, \quad (3)$$

where t is the P-wave traveltime as a function of the offset x, and t_0 is the zero-offset time. Equation 3 can be applied to layered VTI media with the effective parameters given by (Tsvankin, 2005):

$$V_{nmo}^2(N) = \frac{1}{t_0(N)}\sum_{i=1}^{N}\left(V_{nmo}^{(i)}\right)^2 t_0^{(i)}, \quad (4)$$

$$\eta(N) = \frac{1}{8}\left\{\frac{1}{V_{nmo}^4(N)\,t_0(N)}\left[\sum_{i=1}^{N}\left(V_{nmo}^{(i)}\right)^4(1+8\eta^{(i)})\,t_0^{(i)}\right] - 1\right\}, \quad (5)$$

where $t_0^{(i)}$, $V_{nmo}^{(i)}$, and $\eta^{(i)}$ are the interval parameters, and N is the number of layers.

Although the Alkhalifah-Tsvankin equation provides a good approximation for P-wave moveout in VTI media, the trade-off between η and V_{nmo} makes η-estimates highly sensitive to correlated traveltime errors (Grechka and Tsvankin, 1998). In our model, such errors are caused by an isotropic velocity lens in the overburden.

Single-layer model

First, we consider a rectangular lens embedded in a homogeneous VTI layer (Figure 2). Common-midpoint (CMP) gathers were computed with a finite-difference algorithm for a range of lateral coordinates (Figure 3). The lens causes a near-offset time delay of 17 ms and waveform distortions (related to the influence of the side and edges of the lens) in the mid-offset range near the center of the lens (location B).

Using equation 3, we found the best-fit V_{nmo} and η for the target reflector from a 2D semblance scan over the offset range corresponding to spreadlength twice the reflector depth; for comparison, we also performed conventional hyperbolic moveout inversion for the same spreadlength (Figure 4). The NMO velocity estimated from the nonhyperbolic equation outside the lens (location A) is close to the analytic value. At location B, however, V_{nmo} is about 10% greater, although the exact effective NMO velocity estimated from the Dix equation should decrease by 2% due to the low velocity inside the lens. At a

CMP location near the edge of the lens (location C), V_{nmo} is 7% smaller than the exact background value. Interestingly, nonhyperbolic moveout inversion produces a larger error in V_{nmo} than does conventional hyperbolic moveout analysis.

The reason for the lens-induced distortion in V_{nmo} is described in Al-Chalabi (1979) and Biondi (2006) (Figure 5a,b). Near-offset rays at location B pass through the lens twice, while far-offset rays miss the lens completely. Since the lens has a lower velocity, this leads to a smaller traveltime difference between the near- and far-offset traces and, therefore, a higher NMO velocity. In contrast, for location C, the lens is missed by near-offset rays only, and the traveltime difference between the near and far offsets becomes larger, which reduces V_{nmo} (Figure 5b).

The nonhyperbolic inversion gives a better approximation to the actual traveltime due to the contribution of the additional parameter η in the moveout equation. Hence, the fitted nonhyperbolic moveout curve at location B is closer (compared to the hyperbolic equation) to the distorted traveltime curve at near offsets, which causes a pronounced deviation of the estimated V_{nmo} from the exact value (Figure 5c). Note that the velocity V_{nmo} obtained from hyperbolic moveout analysis outside the lens is distorted by the influence of nonhyperbolic moveout.

The obtained laterally varying η-curve resembles the reversed version of the V_{nmo}-curve. While in the absence of the lens the effective η at location B should almost coincide with the background value (0.08), the estimated $\eta = -0.07$ is much smaller. The understated value of η is explained by the need to compensate for the overstated estimate of V_{nmo} in reproducing traveltimes at moderate and large offsets (Grechka and Tsvankin, 1998; Tsvankin, 2005). The magnitude of the η-variation (the difference between the largest and smallest values) along the line is close to 0.3.

One possible approach to mitigate the lens-induced errors is to average the estimated moveout parameters over spreadlength. If the center of the averaging window coincides with the center of the lens, the errors in V_{nmo} and η are reduced to about 1% and 0.02, respectively. However, the errors increase when the averaging window is shifted laterally with respect to the lens. Also, averaging the estimated parameters does not improve the quality of the stacked section and, therefore, cannot replace the correction procedure discussed below.

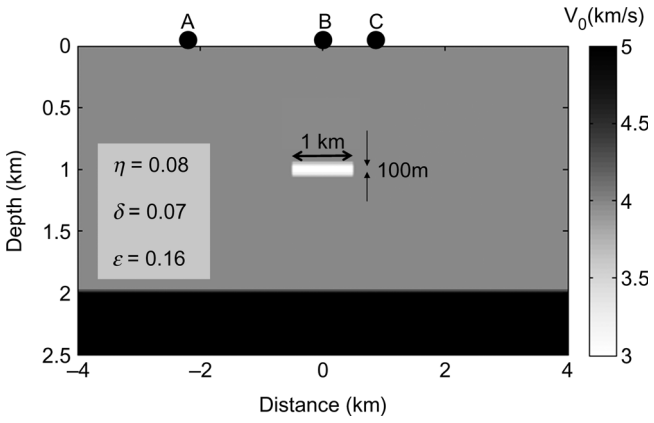

Figure 2. Single VTI layer with an isotropic lens. The lens velocity is 3 km/s; the relevant background parameters are $V_0 = 4$ km/s, $\delta = 0.07$ and $\varepsilon = 0.16$. Points A, B, and C correspond to CMP locations discussed in the text. The test is performed for a spreadlength of 4 km; the target depth is 2 km.

Dependence of distortions on the lens parameters

Next, we investigate the dependence of the inverted moveout parameters on the velocity, width, and depth of the lens using the model in Figure 2. The best-fit parameters V_{nmo} and η are estimated from equation 3 using ray-traced synthetic data. The replacement of finite differences with ray tracing does not significantly change the best-fit parameters.

As expected, the magnitude of the variation in V_{nmo} and η is proportional to the velocity contrast between the lens and the background (Figure 6a). When the spreadlength is fixed, the traveltime distortions depend on the ratio W/L', where W is the width of the lens and L' is the maximum horizontal distance between the incident and reflected rays at the lens depth (Figure 5a). Clearly, L' decreases with the lens depth and goes to zero when the lens is placed at the bottom of the layer. For the model used in the test, the distortions in V_{nmo} and η obtained by nonhyperbolic moveout inversion are largest when the width of the lens is 0.5 km (or $W/L' = 0.25$) (Figure 6b). On the other hand, the error in V_{nmo} estimated from the hyperbolic equation has a relatively flat maximum for the width ranging from 0.5 km to 1.5 km.

As illustrated by Figure 6c, a shallower lens causes larger errors in V_{nmo} and η. For the smallest depth used in the test

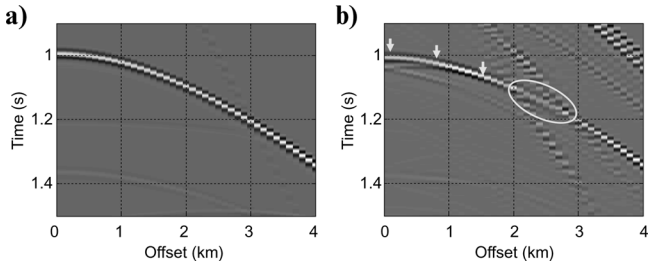

Figure 3. Comparison of CMP gathers for the model from Figure 2 computed with a finite-difference algorithm (a) outside the lens (location A); and (b) above the center of the lens (location B). The traveltime shifts at near offsets (arrows) at location B cause significant errors in the parameters V_{nmo} and η. The distortion produced by the edge of the lens at location B is contoured by the ellipse.

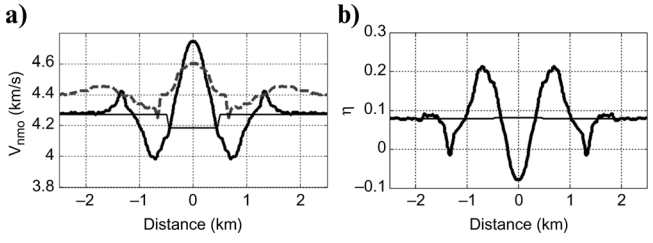

Figure 4. Lateral variation of the inverted (a) V_{nmo} and (b) η (bold solid lines) for the model in Figure 2. The dashed line on plot (a) is the NMO velocity obtained from hyperbolic moveout analysis for the same spreadlength equal to 4 km (the spreadlength-to-depth ratio $X/D = 2$). The exact effective V_{nmo} computed from equation 4 and η computed from equation 5 are marked by thin solid lines.

(0.25 km; $W/L' = 0.29$), the errors are close to the largest distortions for the test in Figure 6b. Note that the ratio W/L' reaches its minimum value (0.25) when the lens is moved up to the surface ($W = 1$ km, spreadlength is 4 km).

Identifying lens-induced distortions

Identifying the range of CMP locations influenced by the lens is critical for avoiding the use of distorted parameters. It is clear from the above results that large variations of V_{nmo} and η on the scale of spreadlength are strong indications of the lens. Numerical tests for the single-layer lens model reveal two additional indicators of the lens — substantial residual moveout after application of nonhyperbolic moveout correction and the dependence of V_{nmo} and η on spreadlength.

The moveout curve distorted by the lens cannot be completely flattened by the nonhyperbolic moveout equation. To estimate the magnitude of the residual moveout, one can use so-called trim statics (Ursenbach and Bancroft, 2001). Trim statics involves cross-correlation between a selected near-offset trace and all other traces, which helps evaluate the statics shifts needed to eliminate the residual moveout. Due to the presence of residual moveout in the area influenced by the lens, application of trim statics increases the semblance (Figure 7). Still, the

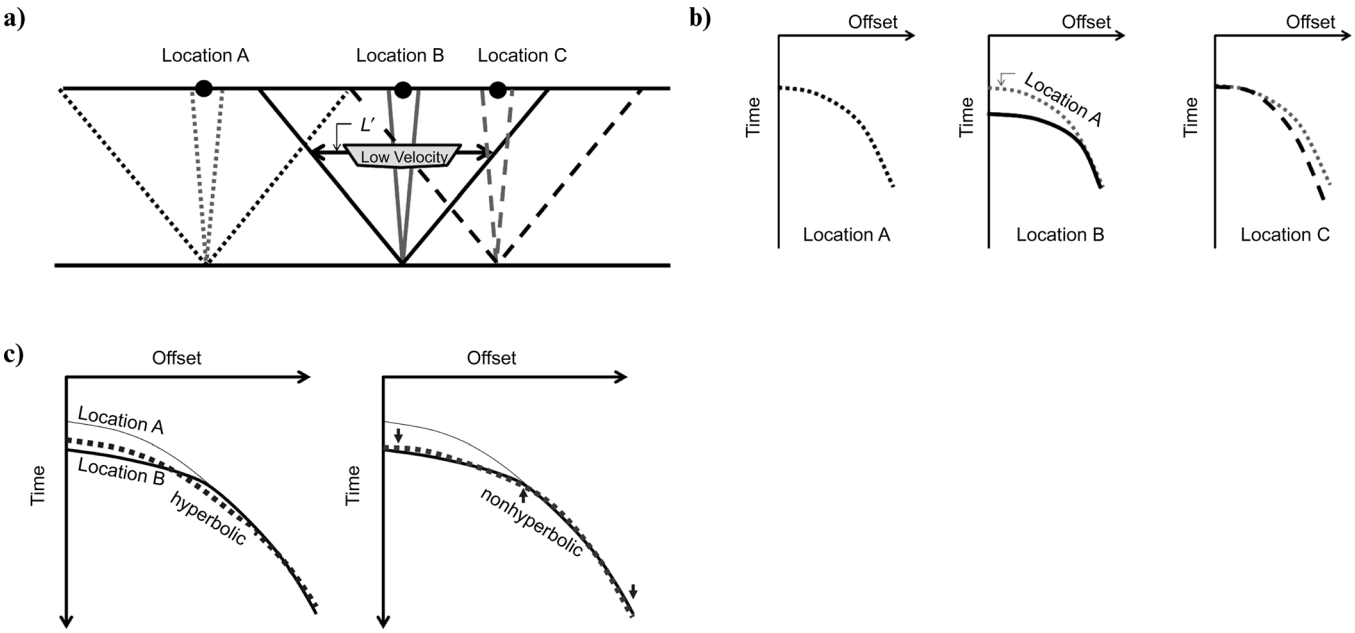

Figure 5. (a) Schematic picture of near- and far-offset raypaths from a horizontal reflector beneath a low-velocity lens at three CMP locations (modified from Biondi, 2006). (b) The influence of the lens on the reflection traveltime. The raypaths and moveout curves at locations A, B, and C are shown by dotted, solid and dashed lines, respectively. (c) Schematic estimated moveout curves (dotted lines) obtained from hyperbolic (left) and nonhyperbolic (right) inversion at location B. The actual moveouts at locations A and B are shown by thin and bold solid lines, respectively.

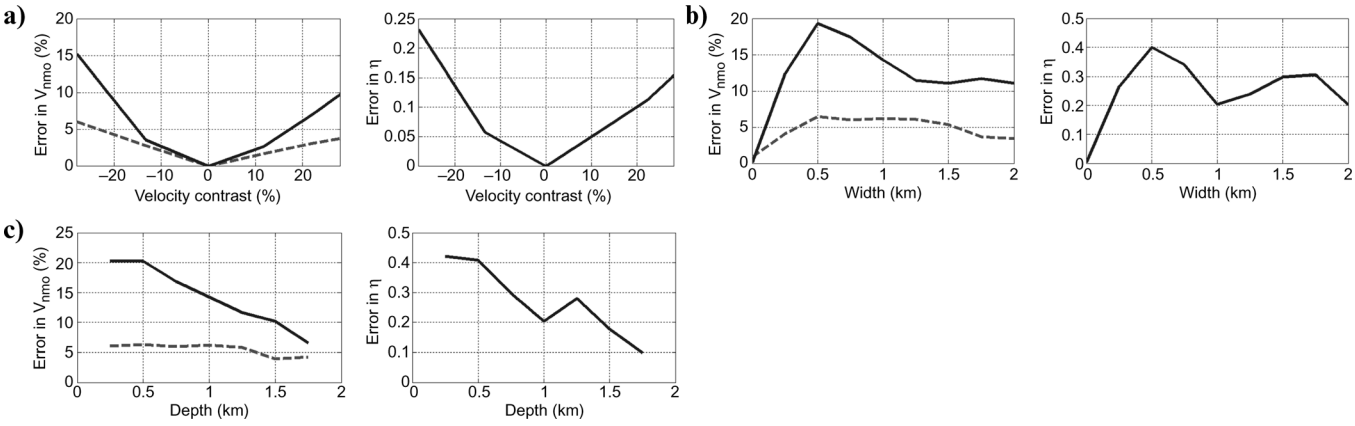

Figure 6. Dependence of the magnitude of the lateral variation in V_{nmo} and η for the model in Figure 2 on (a) the velocity contrast defined as $(V_{lens} - V_{back})/V_{back}$, where V_{lens} and V_{back} are the velocities in the lens and background, (b) the width, and (c) the depth of the lens. V_{nmo} is obtained from nonhyperbolic (solid lines) and hyperbolic (dashed lines) moveout inversion. The spreadlength is 4 km (offset-to-depth ratio $X/D = 2$).

semblance value after application of trim statics at location B is lower than that at location A because of the lens-induced waveform distortions.

Trim statics, however, may not perform well when the data contain random or coherent noise (Ursenbach and Bancroft, 2001). If the signal-to-noise (S/N) ratio is less than five, trim statics increases the semblance by aligning noise components even outside the lens (Figure 7). Thus, trim statics can be used to delineate the area influenced by the lens only for relatively high S/N ratios.

Another possible lens indicator is the variation of the moveout parameters with spreadlength. As shown in Figure 8, the shape of the V_{nmo}- and η-curves is highly sensitive to the spreadlength-to-depth ratio (X/D). In contrast, the estimated moveout parameters at location A outside the lens are much less sensitive to spreadlength when the maximum offset-to-depth ratio lies in the range $1.5 < X/D < 3$.

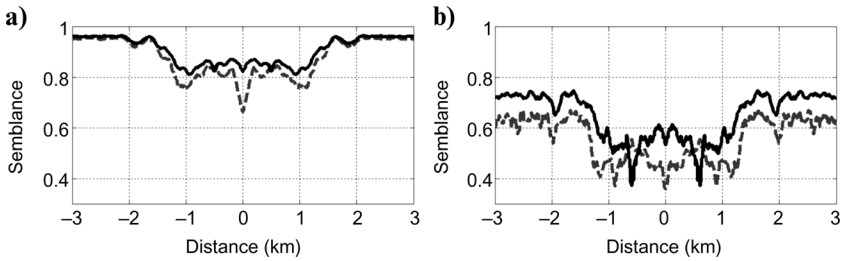

Figure 7. Semblance value for moveout-corrected gathers for the model in Figure 2 before (dashed line) and after (solid line) applying trim statics. The data were contaminated by random noise with the signal-to-noise ratio equal to (a) 10 and (b) 2.

Layered model

The conclusions drawn above remain valid for a more realistic, layered model containing a parabola-shaped lens, which causes a maximum time distortion (or push-down anomaly) of 18 ms (Figure 9). We generated synthetic data with finite differences and applied nonhyperbolic moveout inversion for two interfaces (A and B) below the lens (Figure 10). For a spreadlength of 4 km, the maximum distortion (maximum deviation from the exact value) in V_{nmo} reaches approximately 9% for interface A and 11% for interface B (Figure 10), while η is distorted by up to 0.15 and 0.33, respectively.

The larger errors for interface B are related to its lower ratio X/D. When the spreadlength is increased to 6 km, the errors in V_{nmo} and η for interface B $(X/D = 2)$ decrease to 5% and 0.08, respectively. As is the case for a homogeneous background medium, the moveout-corrected gather exhibits substantial residual moveout in the area influenced by the lens. Thus, the presence of residual moveout after nonhyperbolic moveout correction and the dependence of the moveout parameters on the spreadlength can serve as lens indicators for layered media as well.

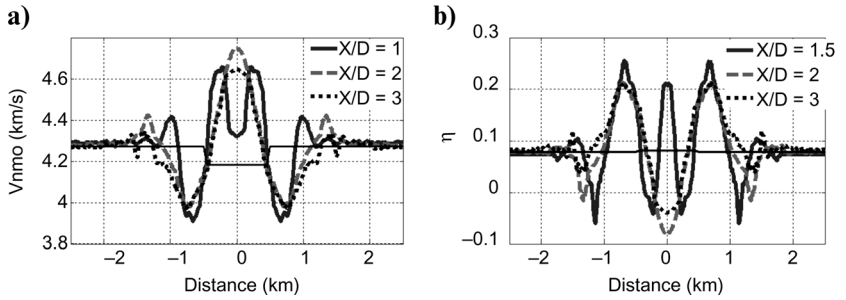

Figure 8. Dependence of the estimated (a) V_{nmo} and (b) η for the model in Figure 2 on the spreadlength-to-depth ratio (X/D).

CORRECTION ALGORITHM

It follows from the modeling results that even a thin lens can cause significant errors in the parameters V_{nmo} and η and an anomaly on the stacked time section. Although the time anomaly becomes smaller if the stack is produced using the background moveout parameters estimated away from the lens, the stacked event then has a smaller amplitude and lower frequency because of a larger residual moveout. Clearly, it is desirable to produce an accurate time section without reducing the quality of the stack.

Here, we introduce two methods for correcting P-wave data from layered VTI media for the influence of the lens. One of them is designed to mitigate the distortions on the stacked section using trim statics. The other method makes it possible to remove the traveltime distortions from each recorded trace and, therefore, obtain both accurate moveout parameters and a high-quality stack.

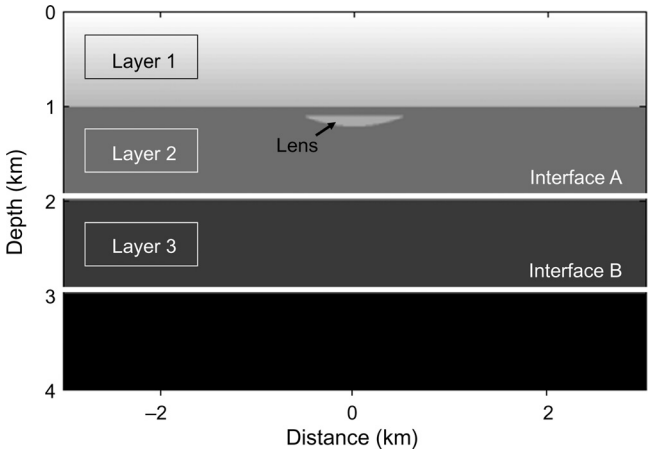

Figure 9. Layered model with a parabola-shaped lens. The first layer is isotropic with a constant vertical velocity gradient; V_0 changes from 1.5 km/s at the surface to 2.5 km/s at the 1 km depth. The second layer is homogeneous VTI with $V_0 = 3.5$ km/s, $\delta = 0.07$, and $\varepsilon = 0.16$ and contains an isotropic lens with $V_0 = 2.7$ km/s. The maximum thickness of the lens is 100 m. The third layer is homogeneous VTI with $V_0 = 4.2$ km/s, $\delta = 0.05$, and $\varepsilon = 0.1$.

Trim statics

By eliminating residual moveout, trim statics makes all traces kinematically equivalent to the zero-offset trace (compare Figure 11b with Figure 11a). Thus, trim statics increases stack power and generates a stack that is kinematically close to the zero-offset section (Figure 11d).

To remove the zero-offset time distortion throughout the section, we assume that the zero-offset raypath is not influenced by the lens and remains vertical for all horizontal interfaces. Then for the model from Figure 9 the distortion of t_0 should be the same at interfaces A and B. This assumption allows us to estimate the push-down anomaly at reflector A and use it for correcting the time distortions for both interfaces. The resulting stacked section is kinematically correct and has a high stack power (Figure 11e). However, as discussed above, trim statics works only for relatively high S/N ratios and cannot be used to estimate the background values of V_{nmo} and η.

Prestack traveltime shifts

The correction algorithm discussed here is designed for a lens embedded in a horizontally layered overburden, but the target reflector can be dipping or curved. Unlike the statics correction, this technique involves computation of traveltime shifts as functions of offset and target depth (Figure 12a). As the input data we use the zero-offset time shifts ("pull-up" or "push-down" anomalies, Δt_0) for the horizontal reflector immediately below

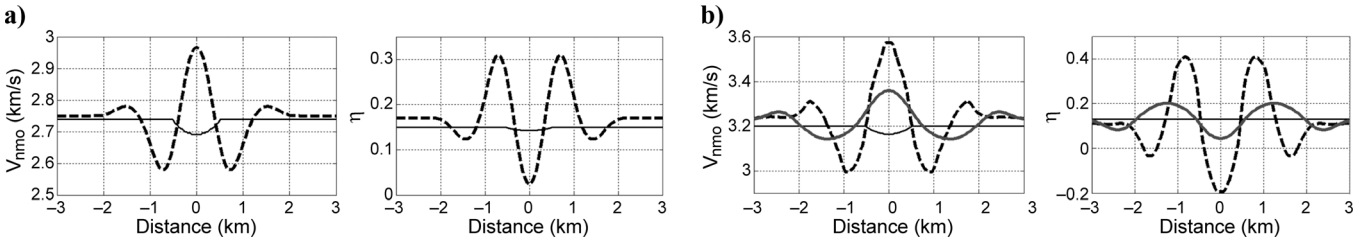

Figure 10. Lateral variation of the estimated V_{nmo} (left) and η (right) for the model from Figure 9 for (a) interface A and (b) interface B. The dashed lines correspond to a spreadlength of 4 km, and the solid lines [only on plot (b)] to a spreadlength of 6 km. The thin solid lines mark the exact parameters.

Figure 11. Moveout-corrected gathers for the model from Figure 9 (a) computed using the best-fit parameters V_{nmo} and η; and (b) after application of trim statics. The stacked section (c) before and (d) after trim statics; (e) the section from plot (d) after removing the push-down time anomaly.

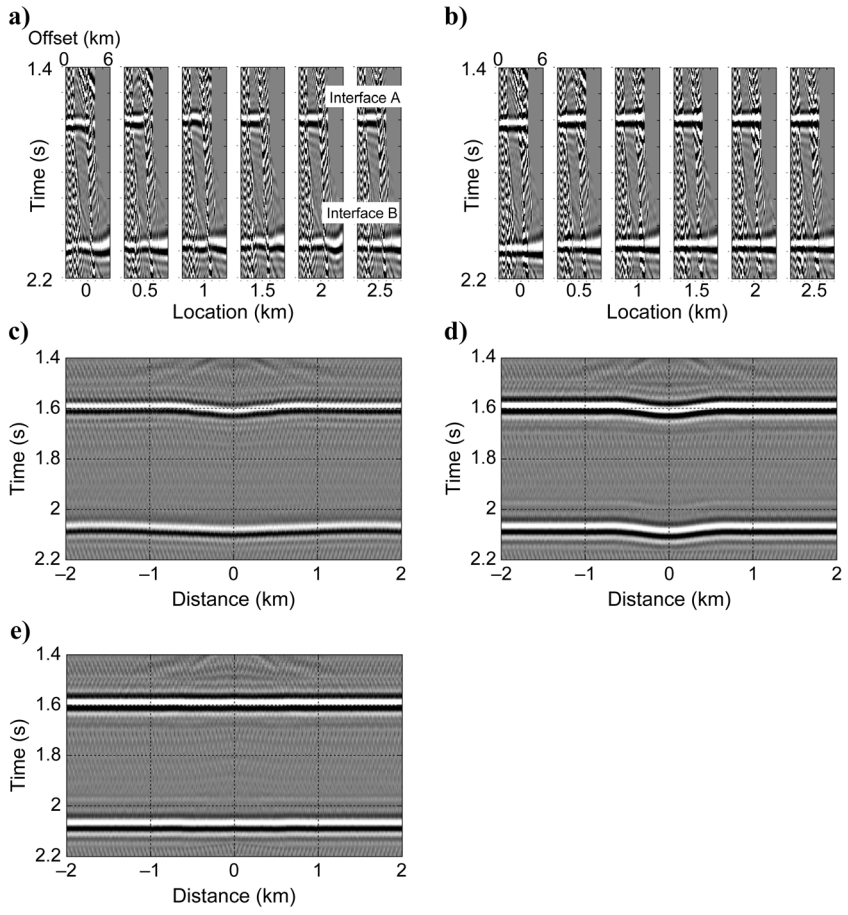

the lens. The lens-related perturbation of the raypath is assumed to be negligible, so that the ray in the layer containing the lens can be considered straight. Then the ray crossing the lens can be reconstructed using the velocity-independent layer-stripping method (VILS) of Dewangan and Tsvankin (2006).

VILS builds the interval traveltime-offset function by performing kinematic downward continuation of the wavefield without knowledge of the velocity field. Each layer in the overburden is supposed to be laterally homogeneous with a horizontal symmetry plane, so that the raypath of any reflection event is symmetric with respect to the reflection point. However, the target interface can be curved and the layer above it can be heterogeneous. Wang and Tsvankin (2009) show that VILS combined with nonhyperbolic moveout inversion provides more robust estimates of the interval moveout parameters in VTI and orthorhombic models than do Dix-type equations.

VILS can be applied to our model under the assumption that the raypath in the overburden is not distorted by the lens. The idea of VILS is to identify reflections from the top and bottom of a certain layer that share the same upgoing and downgoing ray segments. This is accomplished by matching time slopes on common-receiver and common-source gathers; a detailed description of the algorithm can be found in Dewangan and Tsvankin (2006) and Wang and Tsvankin (2009). Matching of the time slopes of the reflections from the target and from the top of the layer containing the lens yields the horizontal coordinates x_{T1} and x_{R1} (Figure 12a). Likewise, the coordinates x_{R2} and x_{T2} are estimated by combining the target event with the reflection from the bottom of the layer containing the lens.

Under the assumption that the lens does not perturb the raypath, we find the horizontal coordinates of the crossing points and the ray angles (Figure 12a,b):

$$x_{TL} = x_{T1} + \frac{z'_{TL}(x_{T2} - x_{T1})}{z}, \tag{6}$$

$$x_{RL} = x_{R1} - \frac{z'_{RL}(x_{R1} - x_{R2})}{z}, \tag{7}$$

$$\cos\theta_{TL} = \frac{z}{\sqrt{(x_{T2} - x_{T1})^2 + z^2}}, \tag{8}$$

$$\cos\theta_{RL} = \frac{z}{\sqrt{(x_{R1} - x_{R2})^2 + z^2}}, \tag{9}$$

where z is the thickness of the layer with the lens, and z'_{TL} and z'_{RL} are the distances between the lens and the top of the layer at locations x_{TL} and x_{RL}, respectively.

If the lens produces a sufficiently strong reflection and the layer is vertically homogeneous, the ratio z'/z can be estimated from the corresponding zero-offset traveltimes (t'/t). For example, in the layered model from Figure 9, we can clearly identify the lens reflection on the stacked section at t = 1.15 s (Figure 13a). This indicates that the horizontal coordinates can be estimated without information about the vertical velocity and anisotropy parameters. Although the ray angles depend on the layer thickness, the algorithm can tolerate realistic uncertainty in the value of z (see below).

The total lens-related traveltime shift for the target event (Δt_{ta}) can be computed as

$$\Delta t_{\text{ta}} = \frac{1}{2}\left(\frac{\Delta t_0(x_{TL})}{\cos\theta_{TL}} + \frac{\Delta t_0(x_{RL})}{\cos\theta_{RL}}\right), \tag{10}$$

where $\Delta t_0(x_{TL})$ and $\Delta t_0(x_{RL})$ are the zero-offset time distortions below the lens at locations x_{TL} and x_{RL}, respectively. Both $\Delta t_0(x_{TL})$ and $\Delta t_0(x_{RL})$ can be estimated from the near-offset stack. The ray angles θ_{TL} and θ_{RL} do not have to be the same, which makes the algorithm suitable for dipping or curved target reflectors.

After the correction, the kinematics of the prestack reflection data should be well-described by the background parameters V_{nmo} and η. The interval values of $V^{(i)}_{\text{nmo}}$ and $\eta^{(i)}$ can be computed using the layer-stripped data corrected for the lens-induced time shifts. The removal of the time distortions should also help generate an accurate, high-frequency stacked section.

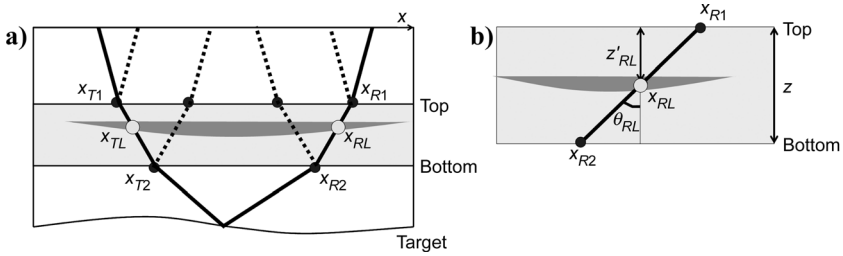

Figure 12. (a) Ray diagram of the correction algorithm. The horizontal coordinates x_{T1}, x_{T2}, x_{R1}, and x_{R2} are determined from the velocity-independent layer-stripping method. (b) Upgoing ray segment crossing the lens. Using the values of z'_{RL} and z, we can compute the horizontal location of the crossing point (x_{RL}) and the ray angle (θ_{RL}).

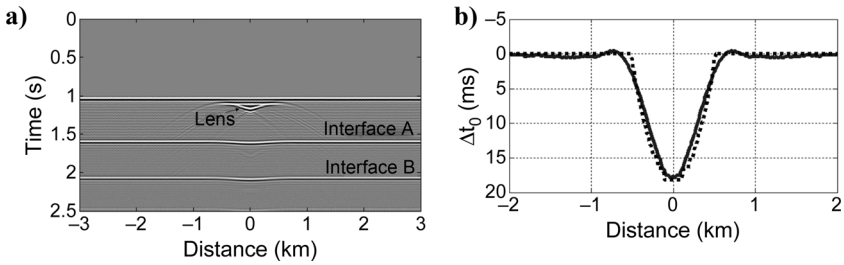

Figure 13. (a) Near-offset stacked section obtained for the offset range from 0 to 200 m, and (b) the magnitude of the push-down anomaly (solid line) estimated by picking the maximum amplitude along interface A. The dotted line in (b) is the exact Δt_0.

Synthetic test

The prestack correction algorithm was tested on the layered model from Figure 9. The required input quantities include the zero-offset time distortion Δt_0, the ratio z'/z, and the thickness z of the layer containing the lens. The values of Δt_0 (Figure 13b) and z'/z (t'/t) were obtained from the near-offset stacked section (Figure 13a). For purposes of this test, the thickness z was assumed to be known.

Application of traveltime shifts computed from equation 10 eliminated the time-varying push-down anomaly and substantially increased the S/N ratio of the stacked section (Figure 14a). Also, the correction significantly reduced the residual moveout in the moveout-corrected gathers (Figure 14b) and the errors in the effective parameters $V_{\rm nmo}$ and η (Figure 15a). For interface B, the distortion in $V_{\rm nmo}$ decreases from 5% to less than 1%, and in η from 0.08 to 0.02. Figure 15b shows that the correction algorithm also produces much more accurate interval parameters $V_{\rm nmo}$ and η estimated from the layer-stripped data. The remaining errors are largely caused by the straight-ray assumption for the layer containing the lens.

It is important to evaluate the sensitivity of the correction algorithm to errors in the input data. Extensive numerical testing showed that as long as the error in Δt_0 is smaller than 25%, the gather produced by equation 10 is sufficiently close to the background reflection traveltime, and becomes almost flat after nonhyperbolic moveout correction. To test the sensitivity to the ratio z'/z, we moved the lens in Figure 9 down by 100 m and 200 m, which corresponds to 10% and 20% errors in z'/z. Although distortions in the moveout-corrected gather become noticeable when the error reaches 20%, the magnitude of the residual moveout is still much smaller than that before application of the time shifts. Finally, a thickness error of up to 20% proved to have little impact on the output of the correction algorithm. An accurate stacked section can be generated even for somewhat larger errors in these input quantities.

DISCUSSION

We proposed an algorithm to correct for the influence of a velocity lens embedded in a horizontally layered overburden. This time-shift technique requires knowledge of approximate values of the zero-offset time anomaly Δt_0, the ratio z'/z, and the thickness z of the lens-containing layer. In the synthetic test, Δt_0 was accurately estimated from the push-down anomaly on the near-offset stacked section, and z'/z was obtained from the corresponding time ratio t'/t using the reflection from the lens (Figure 13).

Although the synthetic model was relatively simple, careful processing of field reflection data often yields sufficiently accurate estimates of the parameters Δt_0 and z'/z. For example, the time section from the central North Sea in Figure 1 contains channel-like structures and pull-up anomalies (see the marked area), which indicate the presence of high-velocity channel fills (Armstrong et al., 2001). The lens reflections are sufficiently strong for estimating the ratio t'/t (and, therefore, z'/z). Whereas the pull-up time anomaly is visible on the full stack, it can be identified much more clearly on the near-offset stacked section (and Δt_0 can be accurately measured). Since in practice depth uncertainty seldom exceeds 20%, errors in z are not expected to cause significant distortions in the correction results.

Our method can also be applied to layered media with multiple lenses, if it is possible to estimate the values of Δt_0 and z'/z for each lens separately. Then the total traveltime shifts

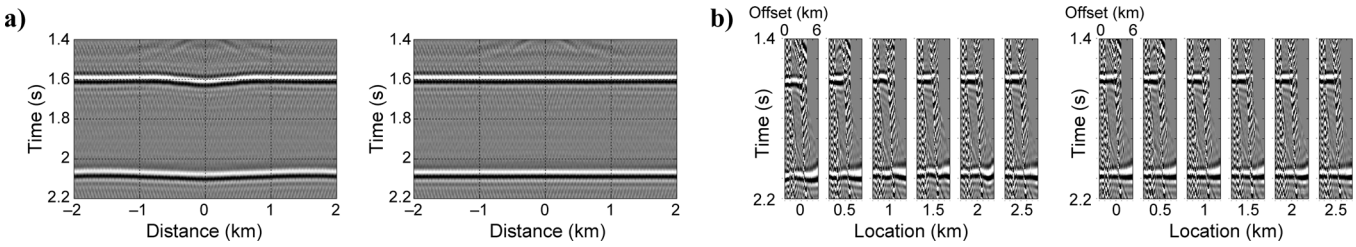

Figure 14. (a) Stacked section and (b) moveout-corrected gathers for the model from Figure 9 obtained before (left plots) and after (right) applying prestack traveltime shifts that compensate for the influence of the lens.

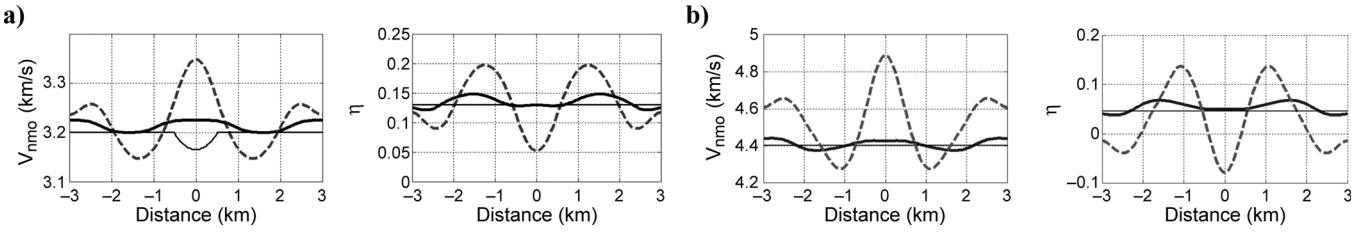

Figure 15. (a) Inverted effective parameters $V_{\rm nmo}$ and η for interface B before (dashed line) and after (thick solid line) applying the correction algorithm. (b) The interval parameters $V_{\rm nmo}$ and η in the third layer (2–3 km) estimated before (dashed line) and after (thick solid line) the correction. The spreadlength (before applying VILS) is 6 km, so for interface B the ratio $X/D = 2$. Thin solid lines mark the exact parameters.

are obtained by summing the individual lens-induced time distortions computed from equation 10. However, the algorithm can break down when a single layer contains multiple lenses or the individual lens reflections cannot be identified. Other key assumptions are those of a laterally homogeneous overburden and straight rays in the layers containing the lenses. Therefore, the correction can become inaccurate when the overburden includes dipping interfaces or has a strong velocity contrast between the lens and the background.

Although the correction method was presented for a 2D model with a single lens, it can be extended to wide-azimuth data from layered media with well-separated multiple lenses. Potentially, the 3D version of the algorithm can be used to correct for the influence of small-scale lateral heterogeneities on azimuthal moveout inversion.

CONCLUSIONS

We demonstrated that a relatively thin velocity lens embedded in a layered VTI medium may cause significant, laterally varying distortions in the moveout parameters V_{nmo} and η estimated from nonhyperbolic moveout analysis. The magnitude of the distortion depends on the width and depth of the lens and is proportional to the velocity contrast between the lens and the background. The error in V_{nmo} is often larger after nonhyperbolic moveout inversion compared with the conventional hyperbolic algorithm applied for the same spreadlength. Hence, although taking nonhyperbolic moveout into account produces smaller residual moveout and higher stacking power, it does not guarantee a more accurate estimation of NMO velocity in the presence of lateral heterogeneity.

Identifying the area influenced by the lens is critical for avoiding use of distorted moveout parameters. We showed that the residual moveout can serve as a lens indicator because the lens-induced distortion cannot be completely removed by nonhyperbolic moveout inversion. The presence of residual moveout can be identified from the increase in semblance after application of trim statics, provided the signal-to-noise ratio is sufficiently high. A lens also manifests itself by making the moveout parameters strongly dependent on spreadlength and CMP coordinate.

To correct for lens-induced traveltime shifts on prestack data, we developed an algorithm based on velocity-independent layer stripping (VILS). Synthetic tests confirmed that the algorithm successfully removes lens-induced distortions on the stacked section and substantially reduces the errors in the effective and interval parameters V_{nmo} and η. The correction requires estimates of the zero-offset time distortion Δt_0, the thickness z of the layer containing the lens and the ratio z'/z, where z' is the distance between the lens and the top of the lens-containing layer. The parameters Δt_0 and z'/z can be obtained from reflection data, while z cannot be found without additional (e.g., borehole) information. However, numerical testing demonstrated that errors up to 20% in Δt_0 and z, as well as a 10% error in the ratio z'/z, do not significantly hamper the performance of the algorithm.

ACKNOWLEDGMENTS

We are grateful to members of the A(nisotropy)-Team of the Center for Wave Phenomena (CWP), Colorado School of Mines (CSM), for helpful discussions. We also thank Tariq Alkhalifah (KAUST, Saudi Arabia), Jeff Shragge (UWA, Australia), and an anonymous referee for their reviews of the manuscript. This work was supported by Japan Oil, Gas and Metals National Corporation (JOGMEC) and the Consortium Project on Seismic Inverse Methods for Complex Structures at CWP.

REFERENCES

Al-Chalabi, M., 1979, Velocity determination from seismic reflection data: Applied Science Publishers.

Alkhalifah, T., 1997, Velocity analysis using nonhyperbolic moveout in transversely isotropic media: Geophysics, **62**, 1839–1854, doi: 10.1190/1.1444285.

Alkhalifah, T., and D. Rampton, 2001, Seismic anisotropy in Trinidad: A new tool for lithology prediction: The Leading Edge, **20**, 420–424, doi:10.1190/1.1438964.

Alkhalifah, T., and I. Tsvankin, 1995, Velocity analysis for transversely isotropic media: Geophysics, **60**, 1550–1566, doi:10.1190/1.1443888.

Armstrong, T., J. McAteer, and P. Connolly, 2001, Removal of overburden velocity anomaly effects for depth conversion: Geophysical Prospecting, **49**, 79–99, doi:10.1046/j.1365–2478.2001.00238.x.

Biondi, B. L., 2006, 3D seismic imaging: SEG.

Blias, E., 2009, Stacking velocities in the presence of overburden velocity anomalies: Geophysical Prospecting, **57**, 323–341, doi:10.1111/j.1365–2478.2008.00750.x.

Dewangan, P., and I. Tsvankin, 2006, Velocity-independent layer stripping of PP and PS reection traveltimes: Geophysics, **71**, no. 4, U59–U65, doi:10.1190/1.2210975.

Fruehn, J., I. F. Jones, V. Valler, P. Sangvai, A. Biswal, and M. Mathur, 2008, Resolving near-seabed velocity anomalies: Deep water offshore eastern India: Geophysics, **73**, no. 5, VE235–VE241, doi:10.1190/1.2957947.

Fujimoto, M., M. Takanashi, M. Szczepaniak, and T. Yoshida, 2007, Application of prestack depth migration across the Ichthys field, Browse basin: ASEG Annual Meeting, Expanded Abstracts.

Grechka, V., 1998, Transverse isotropy versus lateral heterogeneity in the inversion of P-wave reection traveltimes: Geophysics, **63**, 204–212, doi:10.1190/1.1444314.

Grechka, V., and I. Tsvankin, 1998, Feasibility of nonhyperbolic moveout inversion in trans- versely isotropic media: Geophysics, **63**, 957–969, doi:10.1190/1.1444407.

Jenner, E., 2009, Data example and modelling study of P-wave azimuthal anisotropy potentially caused by isotropic velocity heterogeneity: First Break, **27**, 45–50.

Lynn, W. S., and J. F. Claerbout, 1982, Velocity estimation in laterally varying media: Geophysics, **47**, 884–897, doi:10.1190/1.1441355.

Takanashi, M., M. Kaneko, N. Monzawa, S. Imahori, T. Ishibashi, and A. Sakai, 2008, Removal of overburden channel effects through channel velocity modeling and prestack depth migration for an oil field offshore Abu-Dhabi: Abu Dhabi International Petroleum Exhibition and Conference, SPE 117982.

Toldi, J., 1989, Velocity analysis without picking: Geophysics, **54**, 191–199, doi:10.1190/1.1442643.

Tsvankin, I., 2005, Seismic signatures and analysis of reection data in anisotropic media, 2nd ed: Elsevier Science Publishing Company, Inc.

Tsvankin, I., and L. Thomsen, 1994, Nonhyperbolic reection moveout in anisotropic media: Geophysics, **59**, 1290–1304, doi:10.1190/ 1.1443686.

Ursenbach, C. P., and J. C. Bancroft, 2001, Playing with fire: Noise alignment in trim and residual statics: 71st Annual International Meeting, SEG, Expanded Abstracts, 1973–1976.

Wang, X., and I. Tsvankin, 2009, Estimation of interval anisotropy parameters using velocity-independent layer stripping: Geophysics, **74**, no. 5, WB117–WB127, doi:10.1190/1.3157462.

Woodward, M. J., D. Nichols, O. Zdraveva, P. Whitfield, and T. Johns, 2008, A decade of tomography: Geophysics, **73**, no. 5, VE5–VE11, doi:10.1190/1.2969907.